Synthesis and Characterization of Humic Acid-coated Fe_3O_4 Nanoparticles for Methylene Blue Adsorption Activity

Geitu Yirga[1], H C Ananda Murthy[1] and Eshetu Bekele[1,*]

Department of Applied Chemistry, School of Applied Natural Science, Adama Science and Technology University, P.O. Box 1888, Adama, Ethiopia

*Corresponding author: E-mail: eshetubekele@gmail.com

Received: 27 May 2019, Revised: 12 June 2019 and Accepted: 13 June 2019

DOI: 10.5185/amlett.2019.0049
www.vbripress.com/aml

Abstract

Humic acid modified magnetite nanoparticles (HA-Fe_3O_4 NPs) were synthesized by co-precipitation method by varying the precursor magnetite to HA ratio of 10:1 and 20:1. The synthesized NPs were characterized by FTIR, XRD, SEM-EDX and UV-Vis DR Techniques. The appearance of C=O vibration at 1390 cm^{-1} confirms positive interaction of carboxylate anion of HA and Fe_3O_4. The XRD pattern and SEM image shows bare Fe_3O_4 and HA-Fe_3O_4 (10:1 and 20:1) exhibit cubic spinel structure and the spherical shape morphology, respectively. The crystallite sizes of NPs were found to be 11.50 nm, 9.17 nm and 12.65 nm for bare, 10:1 and 20:1 Fe_3O_4-NPs, respectively. The adsorption capacity for the dye was found to increase with increase in contact time, adsorbent dose and initial pH of the solution. The result was best fitted to pseudo 2nd order kinetics model and Langmuir isotherm model. The methylene blue (MB) removal efficiency of bare, 10:1 and 20:1 Fe_3O_4-NPs from aqueous solutions was recorded to be 95.8%, 99.4%, and 97.6%, respectively. The study confirms the greater efficiency of HA-Fe_3O_4 NPs compared to bare Fe_3O_4 for the removal of MB dye. The MB removal efficiency of HA-Fe_3O_4 NPs was found to be proportional to amount of adsorbed HA. Copyright © VBRI Press.

Keywords: Humic acid, magnetite nanoparticles, co-precipitation, methylene blue, adsorption.

Introduction

Organic dyes used in various fields seriously induce water pollution [**1**]. Most of the industrial dyes are toxic, carcinogenic, and teratogenic. Unfortunately, most of them are stable and resistance to photo degradation, biodegradation, oxidizing agents [**2**]. From the different forms of dyes, methylene blue (MB) is a kind of common industrial dyes. It is used for dying wood, silk, and cotton. It is harmful to human beings, animals, and plants. So, the treatment of wastewater containing such a dye is very much significant.

Various methods used for the removal of dyes found to have toxic effects on human beings, animals, plants and the aquatic organisms from industrial effluents [**3**]. Adsorption technique becomes one of the preferable choices to purify the waste water containing dyes. It is reported as more economical, simpler and capable of efficiently treating dyes in more concentrated form than other conventional methods [3, 4]. Moreover, adsorption techniques do not lead to secondary sludge disposal problems [**4**].

Due to the amphoteric nature of magnetite NPs in aqueous media, as a result of deprotonation and protonation, anions and cations can be removed through electrostatic interaction. The non-ionic pollutants can also be adsorbed on the surface of magnetite NPs by physisorption. Recently, magnetic loaded adsorbent materials like iron oxides, have gained special attention in water purification to remove cationic pollutant like heavy metals and dyes. This is due to high separation efficiency, superior magnetic properties; simple manipulation process, mild operation conditions and easy functional modifications [**5**]. Magnetite NPs can be synthesized by different chemical methods like co-precipitation, hydrothermal, micro emulsions, sol gel and thermal decomposition method. whereas magnetite NPs synthesized by co-precipitation method was found to be the simplest, suitable to modify the surface of NPs by insitu synthesis and most efficient chemical pathway to obtain magnetic nanoparticles [**6**].

The main problem associated with magnetite nano particle is its aggregation and oxidation in aqueous solution due to high surface energy, strong magnetic attraction among particles and high van der Waals forces that reduce the removal efficiency of the materials [**7**]. However, these properties can be improved by surface modification with different surface coating materials [**7, 8**].

The coating of surface of the materials makes the material more attractive, easier to use, control particle size, provide different binding site and can be used for a long time [**8**]. Many types of organic materials such as oleic acid (OA) and ethylenediaminetetraacetic acid (EDTA) have been modified at nanoparticles such as coating of Fe_3O_4 nanomaterial to stabilize NMs, and given the nature of some of these capping agents as a result their function groups have adsorptive effect on heavy metal. The present study aimed to use humic acid as coating material to magnetite NPs.

Humic acid is a biopolymer material contains macromolecules with amino acid, amino sugars, peptides, and aliphatic compounds involved in linkages between the aromatic groups and many functional groups like carboxylic, phenol and amine [**9**]. The carboxyl functional group of humic acid binds to magnetite by strong ligand charge reaction and its adsorption modifies the surface charge properties of magnetite based on the amount of adsorbed polyanions [**9, 10**].

Surface modification of Fe_3O_4-NPs particle by coating HA was found to enhance the stability of nano dispersion by preventing their aggregation by electrostatic, steric or combined stabilization layer [**10, 11, 12**]. This led to increase in the absorption capacity of NPs in a wide pH range. Because of this enhanced properties, HA modified magnetite NPs have been extensively used for the removal of heavy metals [**13**], phenol sorption [**14**] and Rhodamine B [**15**]. However, the detailed characterizations of the synthesized materials and its application to remove organic dyes from aqueous solution have not been explored completely. Therefore, in this study humic acid modified magnetite NPs were synthesized, characterized and tested for their adsorption efficiency for methylene blue (MB) removal from aqueous solution.

Experimental

Materials

Chemicals and reagents used in this study includes: $FeCl_3{\cdot}6H_2O$ (Sigma Aldrich), $FeSO_4{\cdot}7H_2O$ (Sigma Aldrich), Methylene blue, ultra-pure ethanol, 25% NH_4OH, NaOH, HCl, NaCl and Humic acid (Sigma Aldrich). All chemicals and reagents used were analytical grades.

Synthesis of Fe_3O_4 and HA-Fe_3O_4 NPs

HA-Fe_3O_4 NPs were prepared by co-precipitation method [**14, 15**]. 6 g of $FeCl_3{\cdot}6H_2O$ and 4 g $FeSO_4{\cdot}7H_2O$ were dissolved in 100 mL water in conical flask and heated to 90 °C for 3 minutes. 15 mL of 25% NH_4OH was added gradually followed by stirring using magnetic stirrer until a black powder was formed in the solution. Then, 0.5 g of HA was dissolved quickly in 50mL of water and added rapidly and sequentially. The mixture was aged at 90 °C for 30 minutes and then cooled down to room temperature. The black precipitate was filtered and washed with water and ultra-pure ethanol and dried in oven at 80 °C for 5h. pH of supernatants was measured using pH meter.

The effect of HA concentration on the surface of magnetite NPs was studied by varying the precursor (Fe3O4-NPs) to HA ratio (10:1) and (20:1). The possible reaction mechanism is as follows:

$$2FeCl_3{\cdot}6H_2O + FeSO_4{\cdot}7H_2O + 8NH_4OH \longrightarrow Fe_3O_4 + 6NH_4Cl + (NH_4)_2SO_4 + 23H_2O \quad (1)$$

$$Fe_3O_4 + HA \longrightarrow Fe_3O_4\text{-}HA \quad (2)$$

Characterization of Fe_3O_4- and HA-Fe_3O_4 - NPs

The crystalline nature of NPs was revealed by X-ray diffraction (XRD) (Shimadzu, XRD-7000S South Korea). Focus Diffractometer with Cu-Kα radiation (λ = 0.15406 nm) operated at 40 kV and 30mA, with a scanning range from 10 °C to 80 °C. Fourier transform infrared (FTIR) spectra of NPs were recorded on Perkin Elmer's spectrophotometer Analyzer using KBr pellets. The surface morphology of NPs was characterized by scanning electron microscope-energy dispersive X-ray spectroscope (SEM- EDX), (Carl Zeiss Model: Neon-40, FESEM/FIB). UV-Vis Diffuse reflectance spectroscopy (UV-Vis DRS, Elico SL-150 spectrophotometer) was used to determine band gap energy using Tauc's equation (3) and optical properties of synthesized NPs. pH meter (HANA Instruments-210) was used for solution pH measurement.

Tauc's equation:

$$\alpha h\upsilon\ 1/n = A(h\upsilon - E_g) \quad (3)$$

where, α is an absorption coefficient constant, hν, is photon energy, E_g is the allowed energy gap, n = ½ for allowed direct transition and n = 2 for allowed indirect transition.

Surface area determination

Surface areas of the NPs were determined according to sear method [**12**]. A 0.5 g of NPs and 10 g NaCl were added in 250 ml conical flask and dissolved by 50 ml of distilled water. Then, the pH of solution was adjusted to 4, and the solutions were titrated by 0.1 M NaOH until pH of the solution reaches to 9. The volume of NaOH required to change pH value from 4 to 9 was recorded. Surface area of the NPs was calculated by the following formula:

$$S = 32V - 25 \quad (4)$$

where, S is specific surface area, V is the volume of NaOH solution in mL

Optimization experiment

The optimization of the experiment was done according to [**11**], by varying the pH (3, 7, 8, 9 and 11), adsorbent dosage (10 mg, 15 mg, 20 mg, 25 mg and 30 mg) and contact time (20 min, 40 min, 60 min, 80, min and 100 min) to get maximum adsorption of the dye by modified nanoparticles. To evaluate the effect of one parameter other parameters were held constant.

Batch adsorption experiment

Batch adsorption experiments were conducted according to [**11, 16**] by varying pH (3, 7, 8, 9 and 11) at optimized adsorbent dosage of 15 mg, optimized time of 60 minute and dye concentration of 25 ml of 10 mg/l. The pH of the solution was adjusted by 0.1M HCl and 0.1M NaOH. The solutions were shaken at room temperature (25℃) with a shaker speed of 100rpm for 60 min; the magnetic nanoparticles were then removed from the solution by using a bar magnet and were filtered with Whatman filter paper of 125 mm size. The absorbance of dyes left in the supernatant solutions after magnetic separation was determined by using UV-Vis spectrophotometer at a maximum wave length of 665nm. The adsorption amount (q_e, $mmolg^{-1}$) of the molecules at the equilibrium step was determined according to the following equation:

$$q_e = \mathbf{V}\ \mathbf{X}\ \frac{\mathbf{Co-Ce}}{\mathbf{M}} \quad (5)$$

$$\%\ Removal = \frac{\mathrm{Co-Ce}}{\mathrm{Co}}\ \mathrm{X}\ 100 \quad (6)$$

where, V is the solution volume (mL); M is the mass of adsorbents (g); and Co and Ce are the initial and equilibrium adsorbate concentrations, respectively.

The kinetics study was conducted at optimum pH of adsorption with the initial dye concentration of (20 mg/L) and (10 mg/L) at fixed adsorbent dosage (25 mg), room temperature (25°C) with shaker speed of 100 rpm and measured at time *t*.

Results and discussion

Characterization

XRD analysis

The XRD patterns of Fe_3O_4, 20:1 and 10:1 NPs were shown in **Fig. 1**. The obtained pattern shows well defined peaks for all the synthesized NPs, confirming their crystalline nature. The characteristic diffraction peaks were seen at 2θ values equal to 30.253°, 35.6055°, 43.8914°, 53.7066° 57.2253°, and 62.8094° which are the reflection of (220), (311), (400), (422), (511) and (440), respectively. Diffraction peaks at d_{311} (2θ = 35.6055°) which were high and sharp observed on all spectra confirms the samples were purely magnetite [**13, 14**].

The XRD peaks observed for synthesized NPs are coherent with the peaks characteristic of inverse cubic spinel structure according to joint committee on powdered diffraction standards of Fe_3O_4 (JCPDS PDF no. 00- 019-0629). The peaks indicated that Fe_3O_4 NPs with a spinel structure and no characteristic peak of impurities were detected in these XRD patterns. The results showed that crystal structure of Fe_3O_4 NPs remain unchanged after being modified using HA. The peak intensities for the HA-Fe_3O_4 NPs were found to be lower than unmodified Fe_3O_4 NPs, which is possibly due to the humic acid coverage at the surface of NPs [**14**]. Because increasing excess amount of humic acid causes decrease in the crystalline nature of nanoparticles which leads amorphous [**17**].

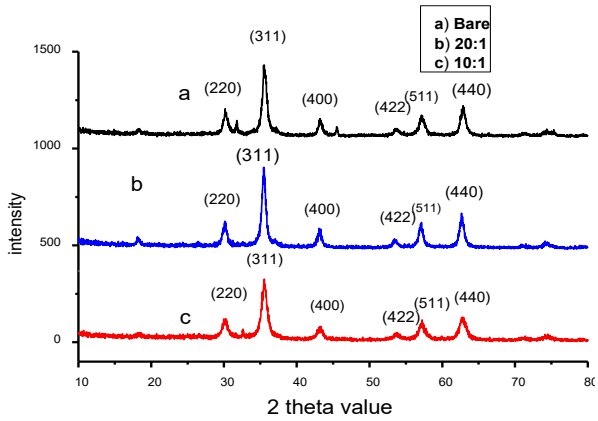

Fig. 1. XRD spectra of (a) bare magnetite, (b) 20:1, and c) 10:1.

The crystallite sizes of the synthesized NPs as calculated using the Debye-Scherer equation (6) were found to be 11.5 nm, 9.17 nm and 12.65 nm for bare magnetite, 10:1 and 20:1 NPs, respectively. This implies increasing HA concentration on the surface of magnetite NPs smaller size crystal was obtained because it enhances crystal growth resulting in smaller size of NPs [**13**]. This effect not observed at lower concentration of HA as in case of 10:1. The small crystallite size obtained for HA coated magnetite NPs confirms its capacity to adsorb the dye molecules more effectively.

FTIR analysis

The FTIR spectra of bare magnetite, 20:1 and 10:1 are given in **Fig. 2**. The broad band around ~3423 cm^{-1} corresponds to O-H stretching indicating the existence of small amount of adsorbed water on NPs [**18**].

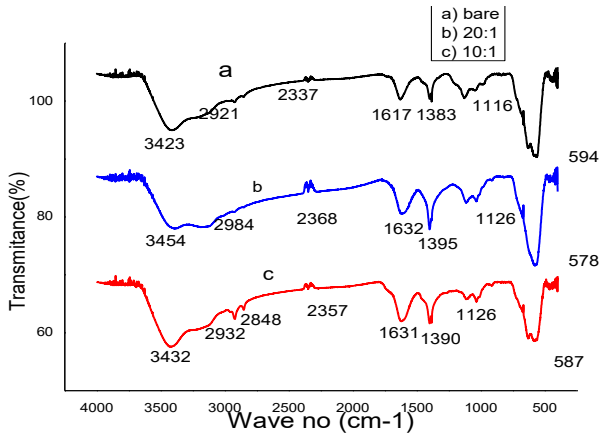

Fig. 2. FTIR spectra of (a) bare magnetite (b) 20:1, and (c) 10:1.

The peak around ~2337 cm^{-1} and 2400 cm^{-1} arises from the absorption of atmospheric CO_2 on the metallic cations [**19**]. The band at ~1617 cm^{-1} could be associated with the bending vibrations of water molecules. The absorption band around ~1400 $cm^{-1}$and 1387 cm^{-1} corresponds to asymmetric stretching of C=O bonds of the CO_2 which might have remained adsorbed on the surface of magnetite during drying. The peak

around ~1129 cm^{-1} and ~1100 cm^{-1} could be due to bending vibration of C=O. The peak appearing at around 594 cm^{-1} is assigned to the metal-oxygen (Fe–O) stretching modes [**20, 21**]. The FTIR spectra of Fe_3O_4 and HA-Fe_3O_4 appeared to be nearly similar but the modified magnetite had a sharp band around 1631cm^{-1}which could be attributed to the presence of –COOH group and aromatic nature of humic acid [**14**]. The peak centered between 578-595 cm^{-1}may be attributed to the stretching vibration of Fe-O bond [**19**]. The successful coating of HA on Fe_3O_4 was revealed by the C=O vibration at 1390 cm^{-1}, indicating that the carboxylate anion interacted with the Fe_3O_4 surface as the C=O vibration in free carboxylate acids is expected around 1700 cm^{-1}. This suggested that carboxylate groups of HA indeed play an important role in the bonding between HA and Fe_3O_4 mainly through ligand exchange [**14**]. These functional groups on the HA-coated magnetite NPs are believed to play significant role during the adsorption of dye.

UV-Vis DRS analysis

As shown in **Fig. 3**, the bare magnetite had the greatest band energy gap of 3.24 eV as compared to HA-Fe_3O_4 where the energy gap was found to be 3.2eV for 10:1 and 3.18 eV for 20:1. This is possibly due to the magnetite surface coverage by coating material HA decreased the incident light absorption by the modified sample [**19**].

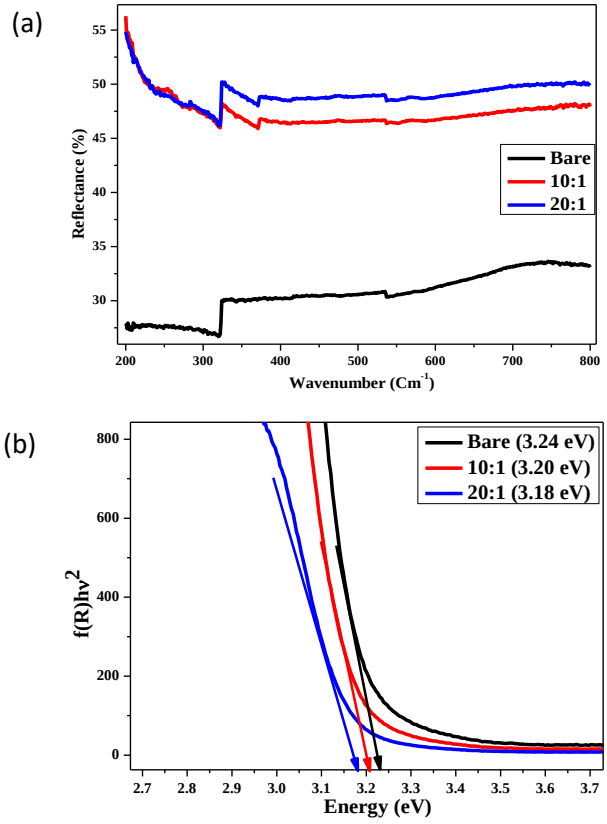

Fig. 3. % of Reflectance of HA-Fe_3O_4 and Fe_3O_4 NPs (a) and Tauc plot from UV-Vis DRS band gap energy of HA-Fe_3O_4 and Fe_3O_4 NPs (b) black color for Bare, red for 10:1, and blue for 20:1.

SEM analysis

The SEM images of bare, 10:1 and 20:1 Fe_3O_4-NPs revealed spherical morphologies as shown in **Fig. 4 (a, b and c)**. The particle size was observed to increase as it is observed from the crystal size in XRD analysis because the XRD analysis done on powdered sample whereas SEM analysis done on solution form which makes little aggregation [**15**]. The HA modified magnetite NPs had a homogeneous surface less aggregated than bare magnetite which is believed to be due to high surface energy of the bare magnetite nanoparticles, but significant agglomeration was found in 20:1 as presented in **Fig. 4c** which is possibly due to small amount of HA slow down crystal growth and high aggregation leading to larger crystal sizes of the NPs.

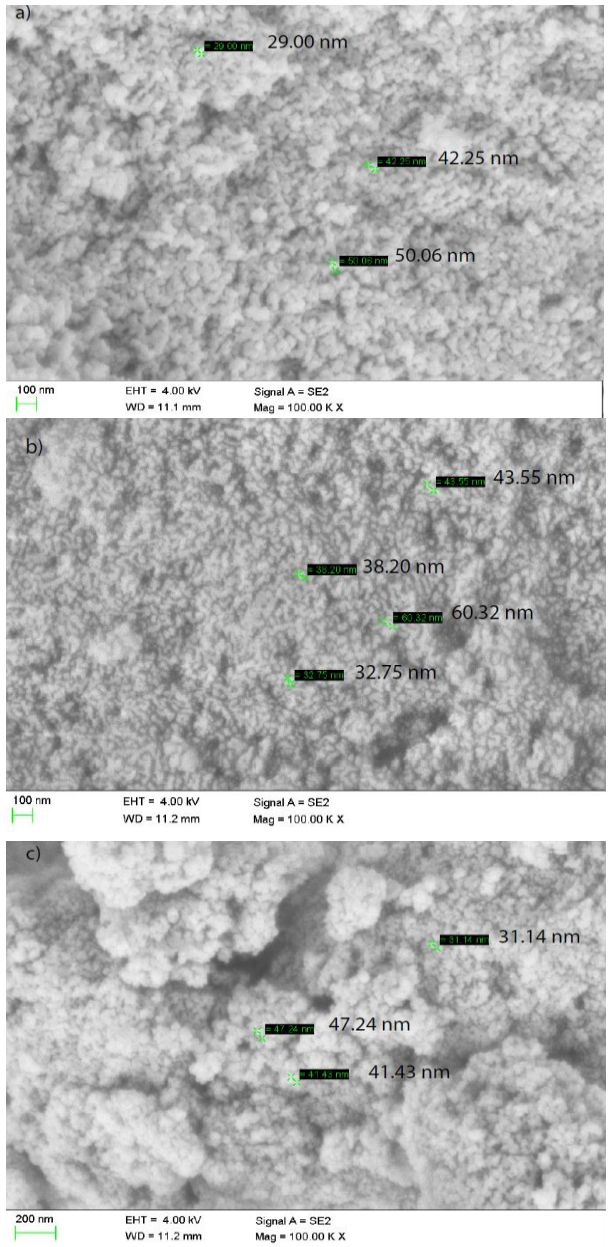

Fig. 4. Scanning Electron Micrograph (SEM) Image of a) Fe_3O_4, b) 10:1, c) 20:1.

EDX analysis

EDX analysis of synthesized NPs showed that strong peaks at 0.8, 6.3, and 6.8 keV confirmed that the presence of Fe in the synthesized NPs, silica (Si) at 1.8 keV, Aluminum (Al) at 1.6 eV and oxygen (O) at 0.8 keV (**Fig. 5**).

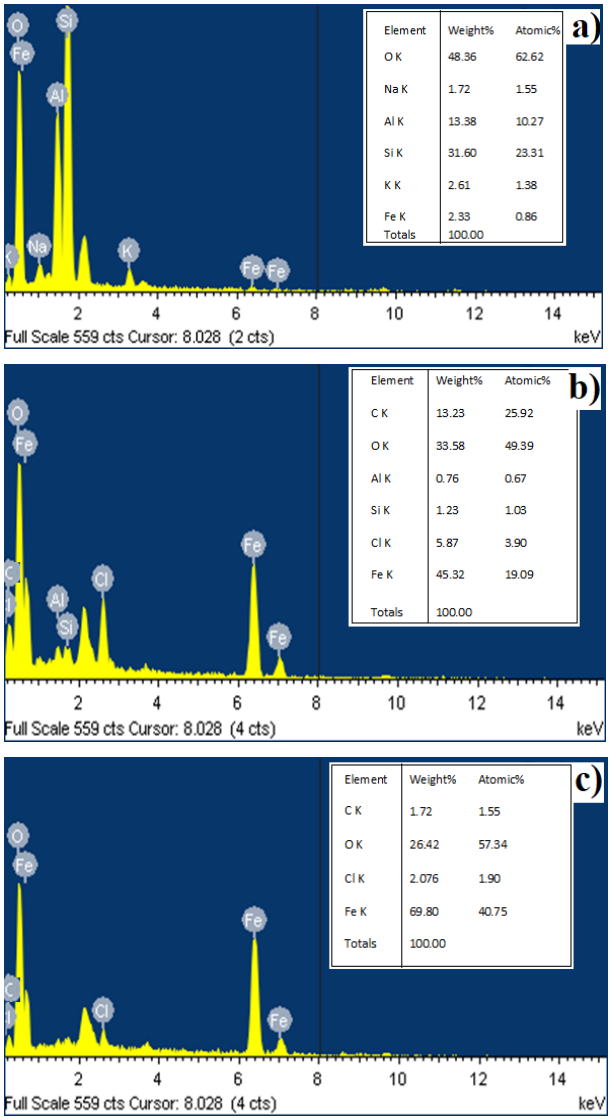

Fig. 5. Energy dispersive x-ray spectra and SEM selected area for EDX analysis of (a) Bare (b) 10:1 and (c) 20:1.

The smaller amount of Si and Al peak were observed due to glass substrate used for film preparation or Detector of EDX. No characteristic peaks of silicon and aluminum was observed from the XRD and FTIR spectra of synthesized NPs. Such types of interference have been viewed by different researchers and it was reported in different literatures [**22**]. The EDX spectrum of HA-Fe_3O_4 NPs showed a carbon signal whereas no carbon signal was observed in case of bare magnetite NPs. The presence of carbon peak as shown in Fig. 4b and c, confirms the effective coating of HA on the surface of magnetite nanoparticles.

Specific surface area

Surface area of the NPs was determined according to sear method. The surface area of 10:1 was found to be greater than 20:1 as shown from the **Table 1**, which could be attributed to the smaller crystal size of 10:1.

Table 1. Sear method surface area calculation.

No.	Type of NPs	Volume of NaOH consumed (mL)	Specific surface area (m^2/g)
1	Bare	8.5	247
2	10:1	10	295
3	20:1	8	231

Adsorption experiment

Effect of pH

The pH of the solution has played a significant role on adsorption of MB on the surface of bare magnetite, 10:1 and 20:1 samples in the pH range of 3-11, as shown in **Fig. 6**. The methylene blue (MB) adsorption capacities were found to increase with increasing solution pH until equilibrium point with pH values of 9, 7 and 9 for bare magnetite, 10:1 and 20:1 respectively. The pH of a medium is a master variable that determines the surface charge of an adsorbent through protonation and de-protonation [**23, 24**]. At acidic pH of 3, MB adsorption was found to be lower which could be attributed to the protonation of anionic groups on 10:1 and 20:1. Bare magnetite resulted in de-protonation of the acid sites on magnetite surface and the surface becoming negatively charged with high attractive properties. This led to increased surface diffusion of the dye molecules due to high electrostatic interactions between MB and magnetite. Lower adsorption of MB at acidic pH might be due to the presence of excess H^+ ions competing with MB cations for the available adsorption sites which reduce the adsorbed amount. Since MB is a cationic dye it removed from the solution on basic medium as shown by previous reports.

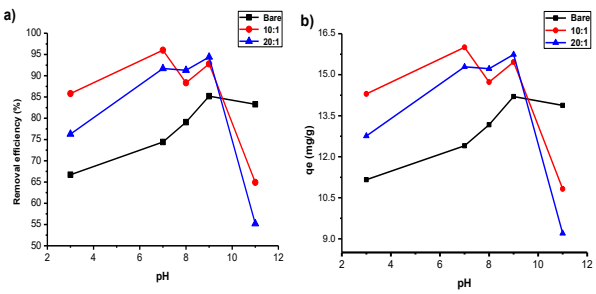

Fig. 6. Effect of pH on (a) MB Removal efficiency (%) of bare and HA-Fe_3O_4 (b) Adsorbent capacity (mg/g) of bare and HA-Fe_3O_4.

Effect of adsorbent dose

The increase in adsorbent dosage found to increase the removal efficiency of MB until equilibrium was

reached (**Fig. 7a**). The methylene blue (MB) removal efficiencies of bare Fe_3O_4, 10:1, and 20:1 from aqueous solutions were recorded to be 95.8%, 99.4%, and 97.6%, respectively at optimum dosage value of 25 mg. Beyond optimum dosage value, the removal efficiency was found to decrease with increase in dosage. This is because increasing the adsorbent reduces the un saturation of the adsorption sites. In addition, overlapping of adsorption sites as a result of over-crowding of adsorbent particles can decrease the removal efficiency of the adsorbent.

As shown in **Fig. 7b**, the adsorption capacity of adsorbents was found to decrease with increasing adsorbent dosage as the number of adsorption sites per unit mass decreases. It has also been observed that HA modified MNPs exhibited higher MB removal efficiency compared with bare magnetite particles because MB binds with the carboxylate group of HA through a proposed ester type linkage, while electrophilic reactions can occur between the nucleophilic functional groups present in HA and the electrophilic MB molecule and through π bonding interactions [**24**].

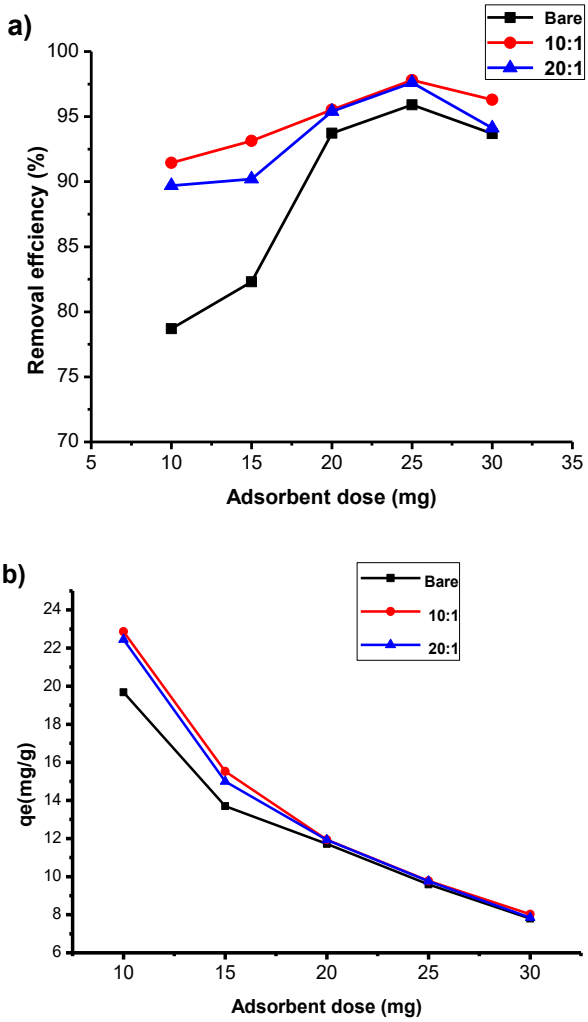

Fig. 7. Effect of adsorbent dosage on (a) MB removal efficiency (%), (b) MB adsorption capacity on adsorbents bare magnetite, and HA-Fe3O4.

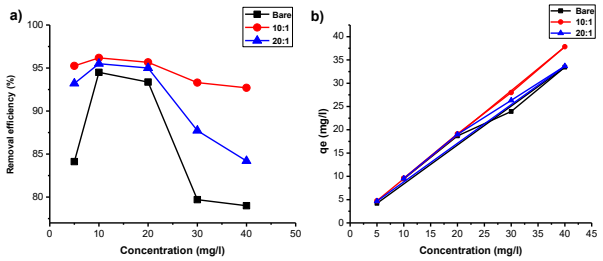

Fig. 8. Effect of initial concentration on (a) MB removal efficiency (%) and (b) Adsorbent capacity (mg/g) for bare magnetite, HA-Fe3O4.

Effect of initial concentration

As shown in **Fig. 8b**, the adsorption capacities of NPs were found to increase with increase in the initial concentration of dye.

However, the percent removal of MB decreases beyond 10 mg/l of dye concentration (**Fig. 8a**) suggesting that the larger ratio of active adsorption sites is available at lower initial concentration that led to the observed greater percentage removal of dye at lower initial concentration but smaller at higher initial concentration. Because with in increasing dye concentration immediately dye adsorbed onto the active site of adsorbent and which prevents further adsorption by repulsion force of dye on the adsorbent phase and on the bulk phase.

Effect of contact time

As shown in **Fig. 9**, the adsorption capacity of adsorbents and percent removal of MB onto the Fe_3O_4 and HA-Fe_3O_4 were found to increase drastically during the initial adsorption stage and then continue to increase at a relatively slow speed with time until a state of equilibrium was attained.

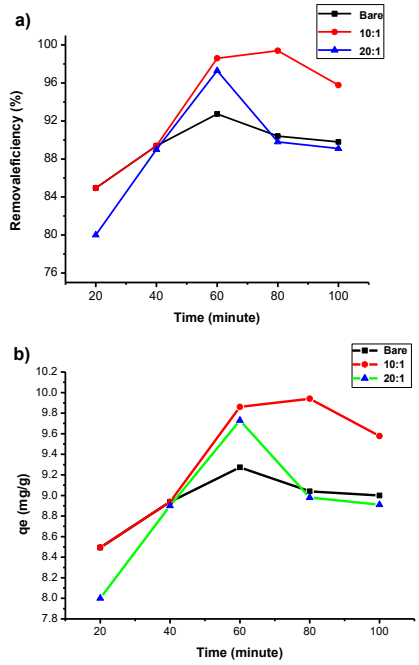

Fig. 9. Effect of contact time on (a) Removal efficiency (%) (b), adsorbent capacity (mg/g)- for bare (unmodified) and HA-Fe_3O_4.

The equilibrium/optimum time was found to be 60 min, 60 min and 80 min for Fe_3O_3, 20:1 and 10:1 with a removal efficiency of 95.8%, 97.8%, and 99.4%, respectively. This phenomenon is attributed to the fact that a large number of vacant surface sites are available for adsorption at the initial stage, and after a lapse of time, the remaining vacant surface sites are difficult to be occupied due to repulsive force between the solute molecules on the solid and bulk [**25**]. As compared to other adsorbents, the synthesized nano adsorbent had high removal efficiency with short equilibrium time. This is due to the high magnetic properties and high aromatic nature of the coating materials [**26**]. As shown in the **Fig. 9**. The equilibrium time for Fe_3O_4 lowers than 10:1 due to smaller number of active site and high magnetic attraction force.

Kinetics study

Kinetic models have been exploited to test the experimental data and to find the mechanism of adsorption and its potential rate-controlling step that include mass transport and chemical reaction. In order to further understand the characteristics of the adsorption process, the pseudo-first-order and pseudo-second-order kinetic models were applied to fit experimental data obtained from batch experiments. The pseudo-first-order and pseudo-second order kinetic models are expressed in linear form as follows;

$$\ln(qe - qt) = \ln Q_e - K_1 t \quad (8)$$

$$\frac{t}{q_t} = \frac{1}{k_2 q_e^2} + \frac{t}{q_e} \quad (9)$$

where, q_e and q_t (mg g^{-1}) are the amounts of MB adsorbed at Equilibrium and at time t (min), respectively. k1 (min^{-1}) is the pseudo-1st-order rate constant and K_2 (g $mg^{-1}min^{-1}$) is the pseudo-2nd-order rate constant. The kinetic parameters and the correlation coefficients (R^2) were determined by linear regression (**Fig. 10** and **11**) and were given in **Table 2**.

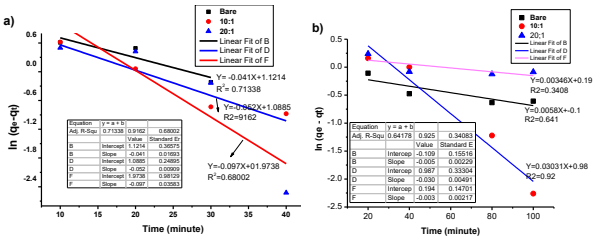

Fig. 10. Pseudo 1st order kinetics (a) at 20mg/l for all (b) at 10mg/l for all adsorbent.

The R^2 values of the pseudo 2nd order kinetic models are much higher than those of pseudo1st-order kinetic model, indicating that the kinetics of MB adsorption follows the pseudo 2ndorder kinetic model. The calculated q_e values (q_e, cal) of pseudo 2nd order models are close to the experimental ones (q_e, exp). All kinetic parameters were calculated from the **Fig. 11** and **Fig. 12** and were given in the **Table 2**.

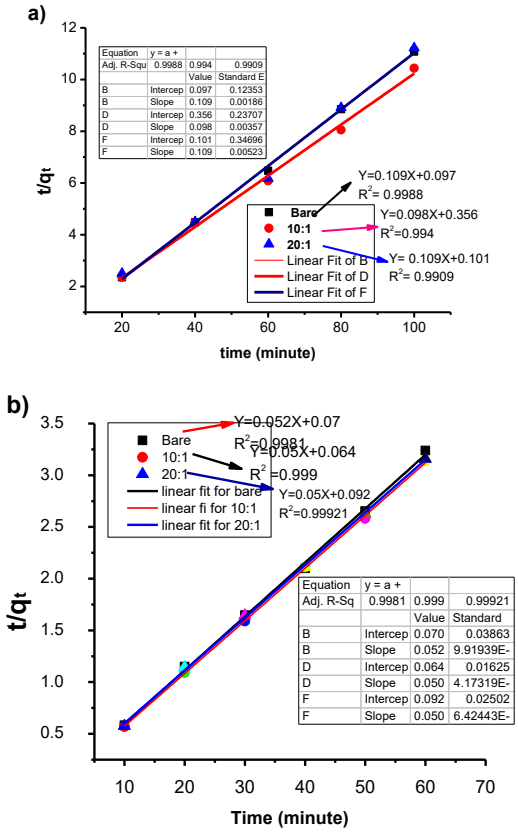

Fig. 11. Pseudo 2nd order kinetics for all adsorbent at (a) 25 ml of 10 mg/l, (b) 25 ml of 20 mg/l concentration.

Adsorption isotherms

In order to evaluate the behavior of molecules of MB with the adsorbent surface, the adsorption isotherms were used to analyze the experimental data. The isotherm provides a relationship between the concentration of dye in solution and the amount of dye adsorbed on the solid phase when both phases are in equilibrium. The most widely used isotherm equations are Langmuir and Freundlich equations [**27, 28**]. The Langmuir model is used to describe the formation of

Table 2. Kinetic parameters for the adsorption of Methylene Blue onto bare Fe_3O_4 and HA-Fe_3O_4 (10:1 and 20:1).

Adsorbents	Concen-tration (mg/l)	Q_e exp. (mg/g)	Pseudo 1st order			Pseudo 2nd order		
			K_1 (min^{-1})	Q_e cal. (mg/g)	R^2	K_2 (min^{-1})	Q_e cal. (mg/g)	R^2
Bare	10	9.273	-0.0058	1.285	0.641	0.1225	9.17	0.998
	20	19.02	-0.041	13.22	0.713	0.03864	19.231	0.998
10:1	10	9.94	-0.030	9.71	0.925	0.027	10.2	0.996
	20	19.356	-0.052	2.97	0.913	0.052	19.607	0.999
	10	9.73	-0.0035	1.564	0.341	0.118	9.17	0.993
20:1	20	19.04	-0.097	94	0.68	0.0283	19.608	0.999

monolayer adsorbate on the outer surface of the adsorbent. The Langmuir isotherm is often applicable to a homogeneous adsorption surface with all the adsorption sites having equal adsorbate affinity, while the Freundlich isotherm described that during the adsorption process different sites of the adsorbent are involved with several adsorption energy is an empirical relation for adsorption over heterogeneous surfaces. Langmuir and Freundlich can be represented in the nonlinear form as follows;

$$\frac{C_e}{q_e} = \frac{1}{q_m b} + \frac{C_e}{q_m} \quad (10)$$

$$\log q_e = \log k_F + \frac{1}{n}\log c_e \quad (11)$$

where, C_e is the equilibrium concentration of solute (mmol L^{-1}), q_e is the amount of solute adsorbed per unit weight of adsorbent (mmol g^{-1} of adsorbate), q_m is the adsorption capacity (mmol g^{-1}), or monolayer capacity, and b is a constant (L $mmol^{-1}$.Where K_f and n are empirical constants incorporating all parameters affecting the adsorption process such as, sorption capacity and sorption intensity respectively. **Fig. 12** and **Fig. 13** shows the equilibrium isotherms for the adsorption of MB onto HA-Fe_3O_4 and Fe_3O_4 NPs. The equilibrium adsorption data was analyzed by using the Langmuir and Freundlich isotherm models respectively.

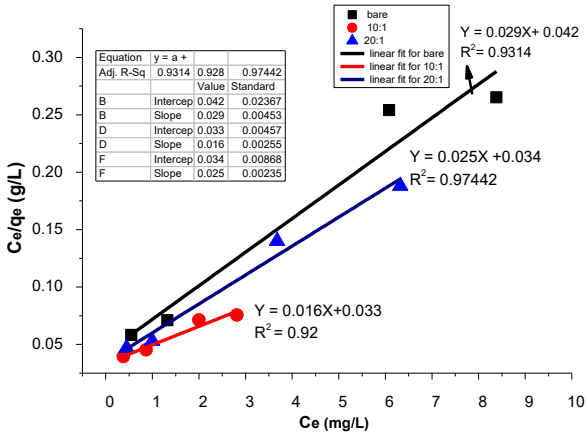

Fig. 12. Langmuir isotherm model for different adsorbents (bare magnetite, 10:1 and 20:1) at constant dosage (25 mg/l), pH optimum (9 for bare and 20:1, 7 for 10:1), contact time 60 min, shaker speed 100 rpm, room temperature and concentration 10-40 mg/l within 10 mg/l intervals.

The essential characteristics of the Langmuir isotherm can be expressed in terms of a dimensionless constant separation factor R_L given by following relation that can be used to determine the feasibility of adsorption in a given concentration range over adsorbent.

$$R_L = \frac{1}{1 + bC_o} \quad (12)$$

where, b is Langmuir constant related to the energy of adsorption (L mg^{-1}) and C_0 is initial concentration (mg/l).

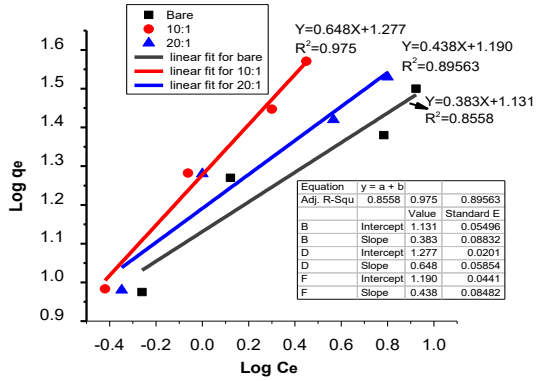

Fig. 13. Freundlich isotherm model for different adsorbents (Fe_3O_4, 10:1 and 20:1) under conditions similar to Langmuir model.

The calculated R_L values at different initial dye concentration were given in the **Table 3.** R_L value indicates the adsorption nature to be either unfavorable if R_L>1), linear if R_L = 1, favorable if 0< R_L<1 and irreversible if R_L = 0 [**29**]. For this study all the valves were lies between 0 and 1 which confirm that the adsorption of dye over the adsorbent was favorable.

Table 3. Calculated R_L values at different initial dye concentration (mg/L) for all adsorbents.

Adsorbents	R_L.values			
	concentration (mg/L)			
	10	20	30	40
Fe_3O_4	0.1266	0.06757	0.0461	0.03497
20;1	0.171	0.0935	0.0643	0.049
10:1	0.11976	0.0637	0.0434	0.0329

The isotherm parameters of both isotherms were calculated and given in the **Table 4**. Based on this the R^2 values of Langmuir model is greater than Freundlich models for bare Fe_3O_4 and 20:1 which indicates that the Langmuir model is suitable for describing the adsorption equilibrium of MB onto these adsorbents but for 10:1 both Freundlich isotherm (**Fig. 13**) and Langmuir model can express the adsorbent behavior but When we see mono layer capacity of adsorbent is greater for Langmuir model and the R^2 value had no significant difference. This signifies that the Langmuir model is suitable for describing the adsorption equilibrium of MB onto this adsorbent.

Table 4. Langmuir and Freundlich isotherm model constants and correlation coefficients for adsorption of MB dye.

Adsorbent type	Isotherm	Regression (R^2)	Estimated isotherm parameters
Bare magnetite	Langmuir	0.954	b = 0.69 L/mg q_m = 34.48 mg/g
	Freundlich	0.903	1/n =0.383, n = 2.61 K_f = 13.52 mg/g
10:1	Langmuir	0.952	b = 0.485 l/mg q_m = 62.5 mg/g
	Freundlich	0.984	1/n = 0.648, n = 1.543 Kf = 18.92 mg/g
10:2	Langmuir	0.982	b = 0.735 l/mg q_m = 40 mg/g
	Freundlich	0.930	1/n = 0.438, n = 2.283 K_f =15.488

Conclusion

Magnetite and humic acid modified magnetite nanoparticles (HA-Fe_3O_4 NPs) were successfully synthesized by coprecipitation method. The method used to prepare the HA-Fe_3O_4 NPs was efficient and humic acid on magnetite NPs was found to prevent the aggregation of magnetite NPs by electrostatic and steric effects as revealed by several characterization results. Moreover, the result confirmed that HA-Fe_3O_4 NPs were found to exhibit high removal capacity of MB dye which could be attributed to the multifunctional and aromatic nature of humic acid. The adsorption kinetics was in good agreement with pseudo 2nd order kinetic equation and the adsorption isotherm showed good fitting to Langmuir equation. The homogeneous surface of HA modified magnetite NPs with less aggregation was revealed by SEM images and thus the HA modified NPs exhibited high removal efficiency. The study confirmed that the dye removal efficiency of HA-Fe_3O_4 NPs depends on the amount of HA adsorbed on the precursor magnetite and it should be optimized for maximum efficiency.

Acknowledgements

The authors gratefully acknowledge Adama Science and Technology University for financial support and laboratory facility to conduct this research work.

References

1. Qu, S.; Huang, F.; Yu, S.; Chen, G.; Kong, J.; *J. Hazard. Mater.*, **2018**, *160*, 643.
2. Ambashta, R. D.; Sillanpaa, M. *J. Hazard. Mater.*, **2010**, *180*, 38.
3. Liu, T.; Li, Y.; Du, Q.; Sun, J.; Jiao, Y.; Yang, G.; Wang, Z.; Xia, Y.; Zhang, W.; Wang, K.; Zhu, H.; Wu, D.; *Colloid. Surface.*, **2012**, *90*, 197.
4. Heidarizad, M.; Şeng, S. S.; *J. Mol. Liq.*, **2016,** 224, 607.
5. Lead, J. R.; Wilkinson, K. J.; *John Wiley, Chichester, UK*, **2006**, 1.
6. Marimón-Bolívar, W.; González, E. E.; *Nanotechnol. Monit. Manage.*, **2018**, *9*, 58.
7. Tipping, E.; Griffith, J. R.; Hilton, J.; *Croat. Chem. Acta*, **1983**, *56*, 613.
8. Dong, F.; Guo, W.; Ha, C. S.; *J. Nanopart. Res.*, **2012**, *14*, 55.
9. Carlos, L.; Cipollone, M.; Soria, D. B.; Moreno, M.S.; Ogilby, P. R.; Einschlag, F. S. G.; Martire, D. O.; *Sep. Pur. Technol.*, **2012**, *91*, 23.
10. Illés, E.; Tombácz, E.; *J. Colloid Interface Sci.*, **2006**, *295*, 115.
11. Qadri, S.; Ganoe, A.; Haik, Y.; *J. Hazard. Mater.*, **2009**, *169*, 318.
12. Hayelom, D.; Nigus, G.; Adhena, A.; *Int. J. Innovation Scientific Res.*, **2014**, *9*, 317.
13. Jing-Fu, Liu; Zong-Shan, Zhao; Gui-Bin, Jiang.; *Environ. Sci. Technol.*, **2008**, *2*, 6949.
14. Andrade, A. L.; Souza, D. M.; Pereira M. C.; Fabris, J. D.; Domingues, R. Z.; *Cerâmica*, **2009**, *55*, 420.
15. Peng, L.; Qui, P.; Lei, M.; Zeng, Q.; Song, H.; Yang, J.; Shao, J,.; Liao, B.; Gu, J.; *J. Hazard. Mater.*, **2012**, *209*, 193.
16. Namasivayam, C.; Sumithra, S.; *J. Environ. Manage.*, ***2005,*** 74**,** 207.
17. Chen, R. P.; Zhang, Y. L.; Wang, X. Y.; Zhu, C. Y.; Ma, A. J.; Jiang, W. M.; *Desalin. Water Treat.*, **2015**, *55*, 539.
18. Maity, D.; Agrawal. *J. Mag. Magn. Mater.*, **2007**, *308*, 46.
19. Chakrabarti, S.; Ganguli, D.; Chaudhuri, S.; *J. Physica.*, **2004**, *24*, 333.
20. Giraldo, L.; Erto, A.; Moreno-Piraján, J. C.; *Adsorption*. **2013**, 19**,** 465.
21. Weber, T. W.; Chakravorti, R. K.; *AIChE Journal*, **1974**, 20, 228.
22. Soerja, K.; Sri Juari, S.; Dwi, S.; Bambang, R.; *Procedia Environment.*, **2017**, 30, 103.
23. Chen, H.; Zhao, J.; Dai, G. L.; *J. Hazard. Mater*., **2011**, 186, 1320.
24. Rashid, M.; Sterbnsiky, G. E.; Pinilla, M. A. G.; Cai, V.; Osha, K. E.; *J. Phys. Chem.*, **2018**, 122, 13540.
25. Wang, M. D.; Zhu, D. Y.; Liu, Y.; Zhang, L.; Zheng, C. X.; He, Z. H.; Chen, D. H.; Wen, L. S.; *Chin. Phys. Lett.* **2008,** 25, 743.
26. Dutta, S.; Bhattacharyya, A.; Ganguly, A.; Gupta, S.; Basu, S.; *Desalination*, **2011**, 275, 26.
27. Abebe, B.; Murthy, H. C. A.; *J. Nanomat.*, **2018**, 10.
28. Hizkeal, T.; Buzuayehu Abebe; Ananda Murthy, H. C.; *Mater. Res. Exp*., **2019**, **6**, 085043
29. Anjaneyulu, Y.; Sreedhara Chary, N.; Suman Raj, D. S.; *Rev. Environ. Sci. Biotechnol.*, **2005**, 4, 245.

